nature geoscience

Article

https://doi.org/10.1038/s41561-025-01735-y

Global-scale shifts in marine ecological stoichiometry over the past 50 years

Received: 23 October 2024

Accepted: 30 May 2025

Published online: 3 July 2025

Check for updates

Ji Liu[1,2], Hai Wang[2], Juan Mou[2], Josep Penuelas[3,4], Manuel Delgado-Baquerizo[5], Adam C. Martiny[6], Guiyao Zhou[5], David A. Hutchins[7], Keisuke Inomura[8], Michael W. Lomas[9], Mojtaba Fakhraee[10], Adam Pellegrini[11], Tyler J. Kohler[12], Curtis A. Deutsch[13], Noah Planavsky[10], Brian Lapointe[14], Yong Zhang[15], Yanyan Li[16], Jiacong Zhou[1], Yixuan Zhang[1], Siyi Sun[1], Yong Li[17], Wei Zhang[16], Junji Cao[17] & Ji Chen[1,18,19]

The elemental stoichiometry of carbon (C), nitrogen (N) and phosphorus (P) regulates marine biogeochemical cycles and underpins the Redfield ratio paradigm. However, its global variability and response to environmental change remain poorly constrained. Here we compile a global dataset of 56,031 plankton (particulate) and 388,515 seawater (dissolved) samples from 1971 to 2020, spanning surface to 1,000 m depth, to assess spatial and temporal dynamics in marine C:N:P ratios. We show that planktonic C:P and N:P, and oceanic C:N and C:P ratios, consistently exceed Redfield ratio throughout the study period, indicating widespread deviation from canonical stoichiometry. Planktonic C:N and N:P ratios rose markedly in the late twentieth century, followed by a decline, suggesting a progressive alleviation of P limitation, probably driven by increased anthropogenic P inputs. Depth-resolved patterns show decreasing oceanic C:N and C:P, and increasing N:P ratios with depth, attributable to differential remineralization and microbial nutrient cycling. Our findings highlight dynamic, non-static stoichiometric patterns over decadal scales, offering critical observational constraints for refining the representation of elemental cycling in biogeochemical models and improving projections of marine ecosystem responses to global change.

Marine carbon (C), nitrogen (N) and phosphorus (P) cycling plays a fundamental role in global ecosystem processes[1,2]. The elemental ratios of C:N:P in plankton (particulate) and seawater (dissolved) are key regulators of material transformation and energy flow in the marine[3,4]. Redfield's seminal work revealed a remarkably consistent elemental composition of marine organic matter, proposing the C:N:P molar ratio of 105:15:1 as a product of marine biological activity[1,2,5]. The average molar ratios of C:N:P in plankton (106:16:1) and ocean (1,017:15:1) have become foundational in oceanography and marine ecology, offering useful baselines and important insights into nutrient dynamics that sustain marine life and drive global biogeochemical cycles[6,7].

However, recent environmental changes may have altered the presumed stability of these ratios[8–10]. The Redfield ratio, derived primarily from North Atlantic observations, may not represent the full spatial and temporal variability of global ocean stoichiometry. For example, planktonic C:N:P ratios show significant latitudinal variation influenced by trophic conditions, and regional studies have increasingly reported deviations from the canonical Redfield ratio[9,10].

Moreover, the influence of seawater depth on stoichiometry is underexplored at the global scale[11,12]. Light availability and nutrient supply vary dramatically with depth, affecting ecological stoichiometry. In the epipelagic zone, high light and low nutrient availability typically

A full list of affiliations appears at the end of the paper. e-mail: chenji@ieecas.cn

lead to elevated C:P and N:P ratios[13–15]. In the mesopelagic zone, where light is scarce and nutrients are redistributed via remineralization and advection, different patterns emerge[13]. Yet, a depth-resolved global synthesis remains lacking.

Ecological stoichiometry in marine ecosystems is shaped by multiple factors, leading to complex temporal trends in C:N:P ratios[12,16]. Increased N and P inputs from atmospheric deposition and riverine fluxes, combined with the relatively constant rate of oceanic C uptake, may contribute to a reduction in oceanic C:N and C:P ratios[17–19] (Extended Data Fig. 1). Conversely, rising carbon dioxide (CO_2) concentrations could increase planktonic C:N and C:P ratios by enhancing C utilization in marine organisms[20,21]. Furthermore, regional variations in nutrient availability, in particular, increasing N and P inputs in Asia, add another layer of complexity to these dynamics[22]. Climate-induced changes such as ocean warming and stratification generally favour higher planktonic C:P ratios, through enhanced C-mobilizing enzyme activity and reduced ribosomal P demand[23,24]. Despite these potential drivers, the factors influencing marine ecological stoichiometry often act in opposing directions, leaving the overall trajectory and magnitude of changes in marine stoichiometry unresolved.

To address these gaps, we compiled an extensive dataset: 56,031 planktonic and 388,515 seawater samples collected globally from 1971 to 2020, across depths from the surface to 1,000 m (Fig. 1). Our study aims to (1) quantify deviations from the Redfield ratio in planktonic and oceanic stoichiometry, (2) identify potential temporal trends in planktonic and oceanic ecological stoichiometry and (3) develop theoretical models to predict changes in planktonic and oceanic ecological stoichiometry across seawater depths.

Shifts in the marine ecological stoichiometry

Our analysis reveals significant global deviations in marine C:N:P stoichiometry from the Redfield ratio across all major ocean basins and depth layers. Planktonic C:P (median 141:1) and N:P (21:1) ratios markedly exceed the canonical Redfield ratios (106:1 and 16:1), consistent across both the epipelagic and mesopelagic zones (Table 1). This deviation is consistently observed across both the epipelagic and mesopelagic zones (Fig. 2a) and across the four major oceans (Extended Data Table 1). The dramatic increase in global P fluxes to the oceans, driven largely by anthropogenic agriculture[25], might suggest a corresponding rise in P assimilation by phytoplankton. However, this is not the case, and may be in part explained by the partial pressure of CO_2 (pCO_2) and rising ocean temperatures[19,20]. Specifically, C and N loading from human activities has surged over the past century—elements that can be sourced from the atmosphere, while P relies primarily on riverine inputs. Consequently, as pCO_2 levels rise, plankton can maintain their C and N balance through enhanced biological N_2 fixation, contributing to the relative scarcity of P and, thereby, elevating the planktonic C:P and N:P ratios[26] (Extended Data Fig. 1). Furthermore, global warming-induced ocean stratification has reduced vertical mixing, limited nutrient transport and further contributed to C-rich conditions[27,28], which elevates the C:P ratio. The shift towards more C-rich planktonic communities has significant implications for the marine food-web structure. Higher C content in primary producers may reduce the availability of P and N for grazers, particularly those with high P and N demands, such as metazoans[12,16]. This imbalance could disrupt trophic interactions and reduce the efficiency of energy transfer across food webs[16]. In addition, the nonlinear effects of rising CO_2 further complicate these dynamics; the rise in ocean temperature can boost respiratory outputs, potentially offsetting the impact of enhanced C fixation and creating a complex feedback loop in marine stoichiometry[20].

Interestingly, the planktonic C:N ratio at depths of 0–1,000 m (6.55:1) closely aligns with the Redfield ratio (6.63:1) (Table 1). This alignment persists across both the epipelagic and mesopelagic zones (Table 1 and Fig. 2a), as well as across the four major oceans (Extended Data Table 1). Despite significant increases in atmospheric CO_2 concentrations since the Industrial Revolution, the global planktonic C:N ratio has remained remarkably stable. Some studies have suggested that increased atmospheric CO_2 concentrations could enhance oceanic C assimilation through photosynthesis and physical uptake, potentially increasing the planktonic C:N ratio[19–21]. For example, in a 25-day large-scale mesocosm experiment in Norway, the uptake of inorganic C by plankton increased by 39% after the CO_2 concentration was increased to 1,050 ppm, and the planktonic C:N ratio could reach 7.5–8.25 (ref. 29). However, our findings suggest that plankton may adjust their metabolism or alter their species composition to adapt to the new environment, such as by increasing biological N_2 fixation from the atmosphere[30], thereby maintaining a relatively stable C:N ratio.

Global oceanic C:N (165:1) and C:P (1919:1) ratios at depths of 0–1,000 m significantly exceed the Redfield ratio by factors of 2.43 and 1.89, respectively (Table 1). These findings support the hypothesis that rising CO_2 levels can elevate oceanic C:N and C:P ratios, contributing to a C-rich epoch in the ocean[20]. Moreover, our analysis reveals an exponential decrease in oceanic C:N and C:P ratios with increasing seawater depth (Fig. 3). In the epipelagic zone, the increases in N and P concentrations (ΔN and ΔP, where Δ denotes changes in elemental stoichiometry with depth relative to surface seawater) are 29 and 57 times greater, respectively, compared with that of C concentration (ΔC). This trend is even more pronounced in the mesopelagic zone, where ΔN and ΔP exceed ΔC by 61- and 91-fold, respectively (Fig. 3a). These asynchronous changes in N and P concentrations also increase the oceanic N:P ratio with increasing seawater depth (Fig. 3b).

A decrease in oceanic C:N and C:P ratios with depth was observed, despite increasing concentrations of C, N and P (Fig. 3). This phenomenon can be attributed to changes in remineralization processes, particle settling kinetics and microbial activity as depth increases. As organic matter sinks through the water column, it undergoes microbial decomposition, releasing C predominantly as volatile CO_2. This diffuses out of the water column more rapidly than N and P, which are released as dissolved inorganic forms such as nitrate and phosphate[26]. In the mesopelagic zone, light availability is severely limited, leading to a near-complete absence of photosynthesis[13]. Consequently, only chemoautotrophic organisms, such as nitrifying archaea and bacteria, contribute to minimal levels of C fixation[15]. In this zone, microbial remineralization processes are slower for N and P compared with C, with N and P being converted to inorganic forms at a much slower rate[31]. This results in the relative accumulation of N and P, leading to higher concentrations of N and P relative to C as depth increases. In addition, the composition of bacterial communities shifts with depth: photosynthetic bacteria dominate in the epipelagic zone, while heterotrophic bacteria, which tend to have higher P quotas, become more abundant in the mesopelagic zone. These heterotrophic bacteria contribute to enhanced respiration, consuming more C and, thus, further reducing the C:P ratio[32]. Moreover, the fraction of detrital C-rich particles increases with depth, and their slower remineralization in deeper waters probably amplifies the relative scarcity of C compared with N and P.

The oceanic N:P ratio increases with depth, primarily due to differential remineralization rates and microbial activity (Fig. 3). As organic matter descends through the water column, it undergoes microbial decomposition, releasing dissolved inorganic nutrients such as nitrate and phosphate. P is generally remineralized more efficiently and rapidly than N, resulting in relatively higher P concentrations at shallower depths and lower concentrations at greater depths[32]. Moreover, as oxygen levels decrease with depth, denitrifying bacteria reduce nitrate to N gas, further decreasing the available N pool in deep waters. This process further elevates the relative abundance of P, contributing to the observed trend of increasing N:P ratios with depth[33].

In contrast to the significant variability observed in oceanic C:N:P ratio with increasing seawater depth, planktonic C:N:P ratios remain

https://doi.org/10.1038/s41561-025-01735-y

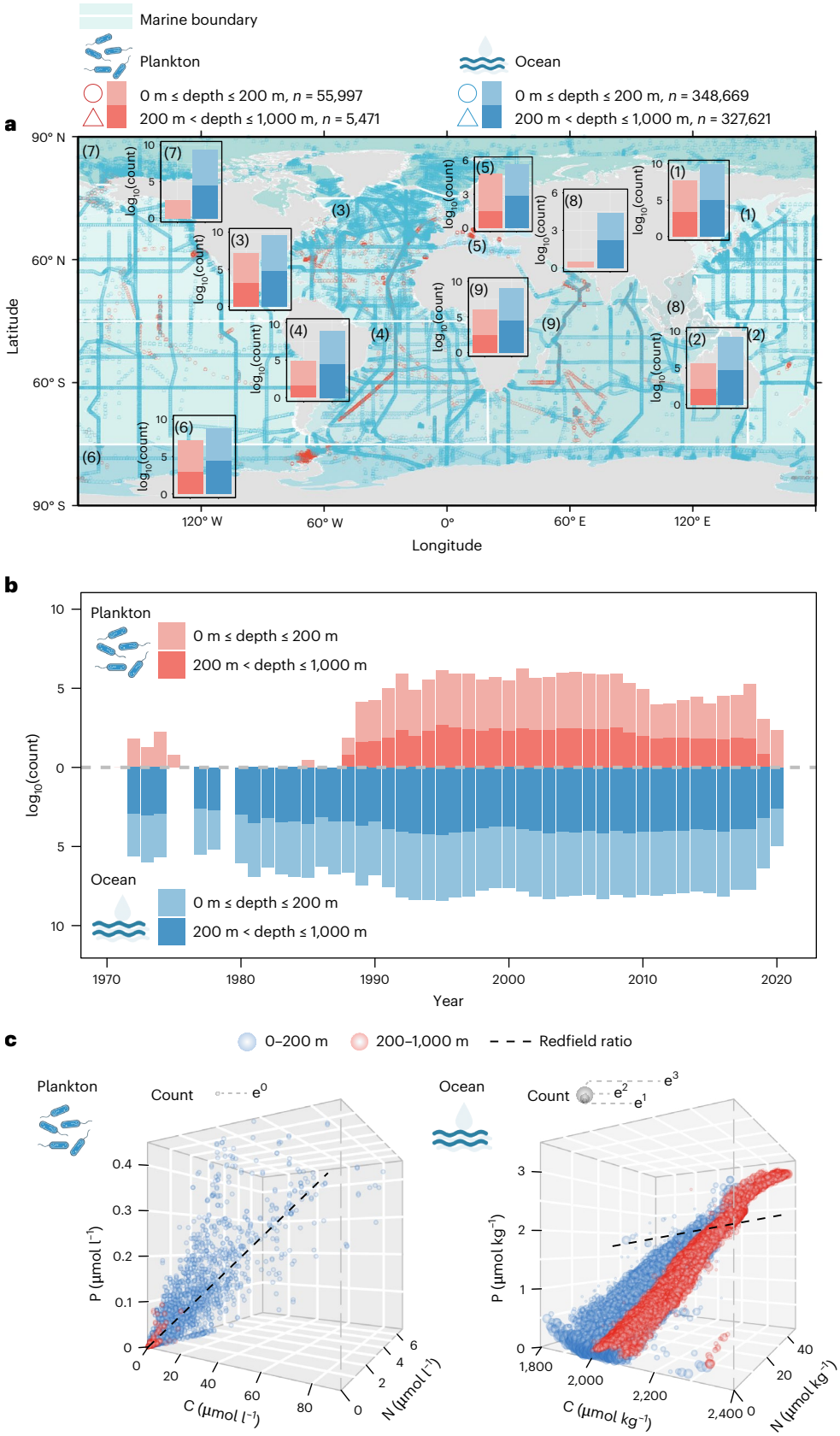

Fig. 1 | Global marine ecological stoichiometry patterns. a–**c**, Spatial (**a**), temporal (**b**) and ecological stoichiometry (**c**) patterns of globally sampled plankton and oceans. Sampling depths were divided into two intervals: epipelagic (0 m ≤ depth ≤ 200 m) and mesopelagic (200 m < depth ≤ 1,000 m). The delineation of marine regions adhered to categorizations defined by the International Hydrographic Organization and the Flanders Marine Institute (https://www.marineregions.org/): (1) North Pacific Ocean, (2) South Pacific Ocean, (3) North Atlantic Ocean, (4) South Atlantic Ocean, (5) Mediterranean Region, (6) Southern Ocean, (7) Arctic Ocean, (8) South China and Eastern Archipelagic Seas and (9) Indian Ocean. 'e' refers to the base of the natural logarithm, an irrational number approximately equal to 2.71828. The utilized dataset is delineated in Supplementary Table 1.

Table 1 | A summary of the ecological stoichiometric ratio for plankton and ocean globally across different depth ranges

Depth (m)	Seawater analyses	C:N (molar ratio)			C:P (molar ratio)			N:P (molar ratio)		
		Values (95% CI)	Redfield ratio	*P*	Values (95% CI)	Redfield ratio	*P*	Values (95% CI)	Redfield ratio	*P*
0–200	Plankton	6.53 (6.51–6.54)	6.63	***	141 (140–142)	106	***	20.8 (20.6–21.0)	16.0	***
	Ocean	231 (228–234)	67.8	***	3,314 (3,286–3,340)	1,017	***	12.6 (12.5–12.6)	15.0	***
	Biological activity	5.83 (5.80–5.86)	7.00	***	91.6 (91.1–92.0)	105	***	12.5 (12.5–12.5)	15.0	***
200–1,000	Plankton	7.07 (6.97–7.17)	6.63	***	127 (117–136)	106	***	22.3 (20.1–25.0)	16.0	***
	Ocean	103 (101–104)	67.8	***	1,172 (1,167–1,179)	1,017	***	14.2 (14.2–14.3)	15.0	***
	Biological activity	6.19 (6.17–6.22)	7.00	***	85.2 (85.0–85.4)	105	***	14.0 (14.0–14.0)	15.0	***
0–1,000	Plankton	6.55 (6.54–6.57)	6.63	***	141 (140–142)	106	***	20.8 (20.6–21.0)	16.0	***
	Ocean	165 (164–166)	67.8	***	1,919 (1,909–1,929)	1,017	***	13.7 (13.6–13.7)	15.0	***
	Biological activity	6.33 (6.31–6.35)	7.00	***	97.4 (97.1–97.6)	105	***	13.3 (13.3–13.3)	15.0	***

The values for plankton and ocean are the median of the elemental ratios. The value for biological activity is the slope of the fit representing the ratio of changes in elemental concentrations due to biological activity. Values in parentheses are 95% confidence intervals (CI). The Wilcoxon rank-sum test (two-sided) was used for statistical testing, with computational details for confidence intervals and *P* provided in the Methods. ***$P < 0.001$.

remarkably stable (Fig. 3 and Extended Data Fig. 2). Plankton achieve this stability through intricate physiological adjustments that compensate for the large variations in light and nutrient availability encountered with depth. Phytoplankton, being more flexible, can adjust their internal stoichiometric content in response to changing environmental conditions[11]. By contrast, zooplankton, while capable of adjusting their stoichiometric composition to some extent, are generally less flexible than phytoplankton[34]. Furthermore, zooplankton often migrate vertically in response to environmental changes, which influences their exposure to different nutrient and light conditions. These organisms optimize light energy utilization by modulating the synthesis of photosynthetic proteins and pigments in response to low-light conditions[35]. Moreover, nutrient storage and utilization are tightly regulated: under N scarcity, plankton increase carbohydrate and lipid storage, while in P-limited environments, they reduce ribonucleic acid synthesis to conserve P (ref. 36). Adaptations in cell size and morphology also play a critical role, with smaller cells predominating in nutrient-rich shallow waters and larger cells more common in deeper, nutrient-scarce zones[26]. Moreover, plankton adjust their metabolic pathways and reallocate biochemical components in response to nutrient availability, thus ensuring efficient resource use[36]. These physiological strategies are further reinforced by the regulation of gene expression and enzyme activities, optimizing photosynthesis and nutrient metabolism across varying environmental conditions[37]. Collectively, these adjustments enable plankton to maintain a stable C:N:P ratio across different depths, facilitating their survival and growth in diverse marine environments.

Temporal dynamics for marine ecological stoichiometry

Contrary to existing paradigms, our analyses further indicate that global marine ecological stoichiometry changes over time rather than remaining static (Fig. 4). Planktonic C:P and N:P ratios showed significant temporal fluctuations, increasing steadily from 1970 to 2007, and converging towards median values of C:P (141:1) and N:P (21:1) observed in the epipelagic zone (Fig. 4a). This temporal trend is particularly evident in the Pacific and Atlantic Oceans, although a lack of sufficient time-series data limits the analysis in the Indian and Arctic Oceans (Extended Data Figs. 3–6). The increasing C:P and N:P ratios suggest a trend towards P limitation, probably driven by adaptations to elevated pCO_2 levels, which enhance C assimilation and stimulate biological N_2 fixation, thus maintaining the balance of C and N while exacerbating P limitation[20]. The relatively limited availability of P from terrestrial sources, in contrast to the more abundant atmospheric sources of C and N, further contributes to the rising planktonic C:P and N:P ratios, particularly in the presence of sufficient micronutrients such as iron[24].

In the early twenty-first century, however, planktonic C:P and N:P ratios exhibited a declining trend (Fig. 4a). The intensification of soil erosion and weathering, exacerbated by increased tillage and climate warming, has led to higher annual inputs of P from terrestrial to marine systems, alleviating P limitation[25,38]. Integrated modelling studies also project a decline in the inorganic N:P ratio of terrestrial inputs to the ocean, with predictions suggesting changes in these inputs could range from −2% to 9% for N and 37% to 57% for P between 2000 and 2050 (ref. 39). Recent observational data corroborate these findings, indicating increased P inputs from the Amazon River to the Atlantic Ocean, which have alleviated P limitation in the tropical Atlantic and Caribbean Sea, contributing to the formation of *Sargassum* blooms since 2011 (refs. 40,41). These findings suggest that the rising terrestrial P inputs to the ocean in the early twenty-first century may alleviate P limitation in plankton, potentially leading to declines in planktonic C:P and N:P ratios.

While previous biogeochemical models predict an increase in phytoplankton P limitation, our observations of a decline in planktonic C:P and N:P ratios between 2007 and 2020 present a potential conflict[42]. One possible explanation for this discrepancy is that models may underestimate P inputs or fail to incorporate the full range of environmental factors influencing nutrient cycling. These models typically assume consistent nutrient availability and fixed stoichiometry, but real-world variations in nutrient loading, atmospheric deposition and the complex dynamics of climate change may lead to different outcomes. Our findings suggest that the P limitation hypothesis may need to be revisited, especially when considering the multifaceted nature of marine biogeochemical processes. A more recent model[43] shows that the P is rarely limited, at least primarily, in the ocean, consistent with the compiled observations[44]. As a result, the P storage capacity of individual taxon has a substantial impact on planktonic C:P and N:P ratios[43]. At the same time, C:P and N:P ratios may also be impacted by the dissolved P concentration, especially when the concentration is low[43]. Thus, the combination of change in oceanic P concentration and community shift at the observed locations could explain the temporal shift in C:P and N:P ratios. Even if the oceanic P concentration increases, this effect on the planktonic C:P and N:P could be overwhelmed by that of the community shift.

The exception is the global planktonic C:N ratio, which shows no significant temporal trend from 1970 to 2020 in either the epipelagic or mesopelagic zones (Fig. 4a). The homeostasis observed in the planktonic C:N ratio supports the hypothesis that plankton are capable of maintaining a stable C and N balance through metabolic regulation[6]. This homeostasis, evident across large spatial and temporal scales, indicates a strong resilience to environmental perturbations.

https://doi.org/10.1038/s41561-025-01735-y

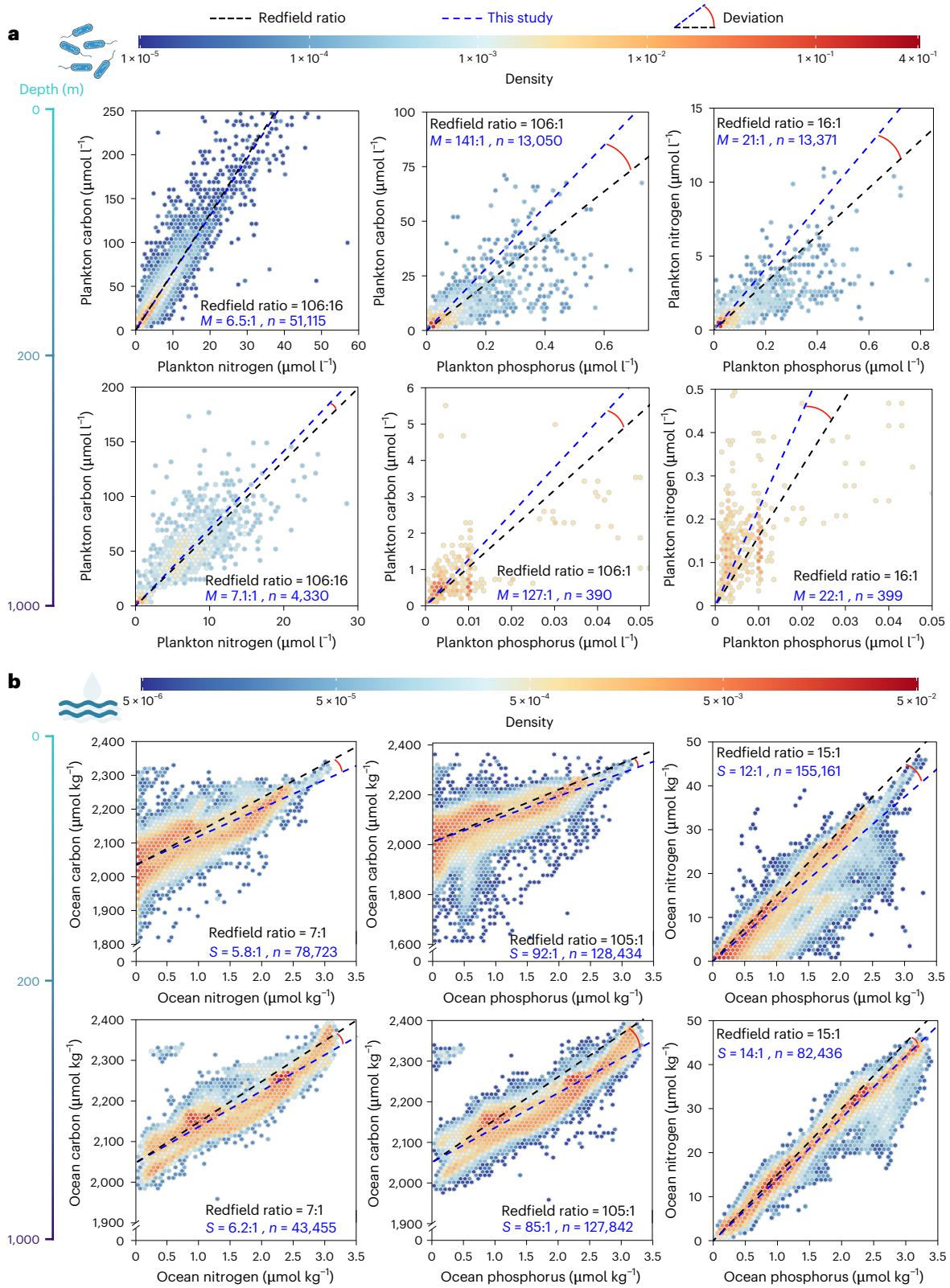

Fig. 2 | Distributions of C, N and P concentrations in planktonic and oceanic environments. a,**b**, Planktonic (**a**, n = 56,031, particulate) and oceanic (**b**, n = 388,515, dissolved) concentrations of C, N and P. The dashed black lines indicate the Redfield ratio (**a**, 106:16:1) and changes due to biological activity (**b**, 105:15:1). Density represents the distribution frequency of each subgraph sample, and the sum of the densities of all the pixels in each subgraph equals 1. M, median; S, slope; n, sample size.

Although the oceanic C:N ratio remains higher than the Redfield ratio, it has shown relative stability since the early twenty-first century (Fig. 4b). This suggests that plankton actively regulate their C:N ratio in response to elevated atmospheric pCO_2 levels by modulating growth and metabolic processes, thereby contributing to the overall stability of marine ecological stoichiometry. Through photosynthesis

https://doi.org/10.1038/s41561-025-01735-y

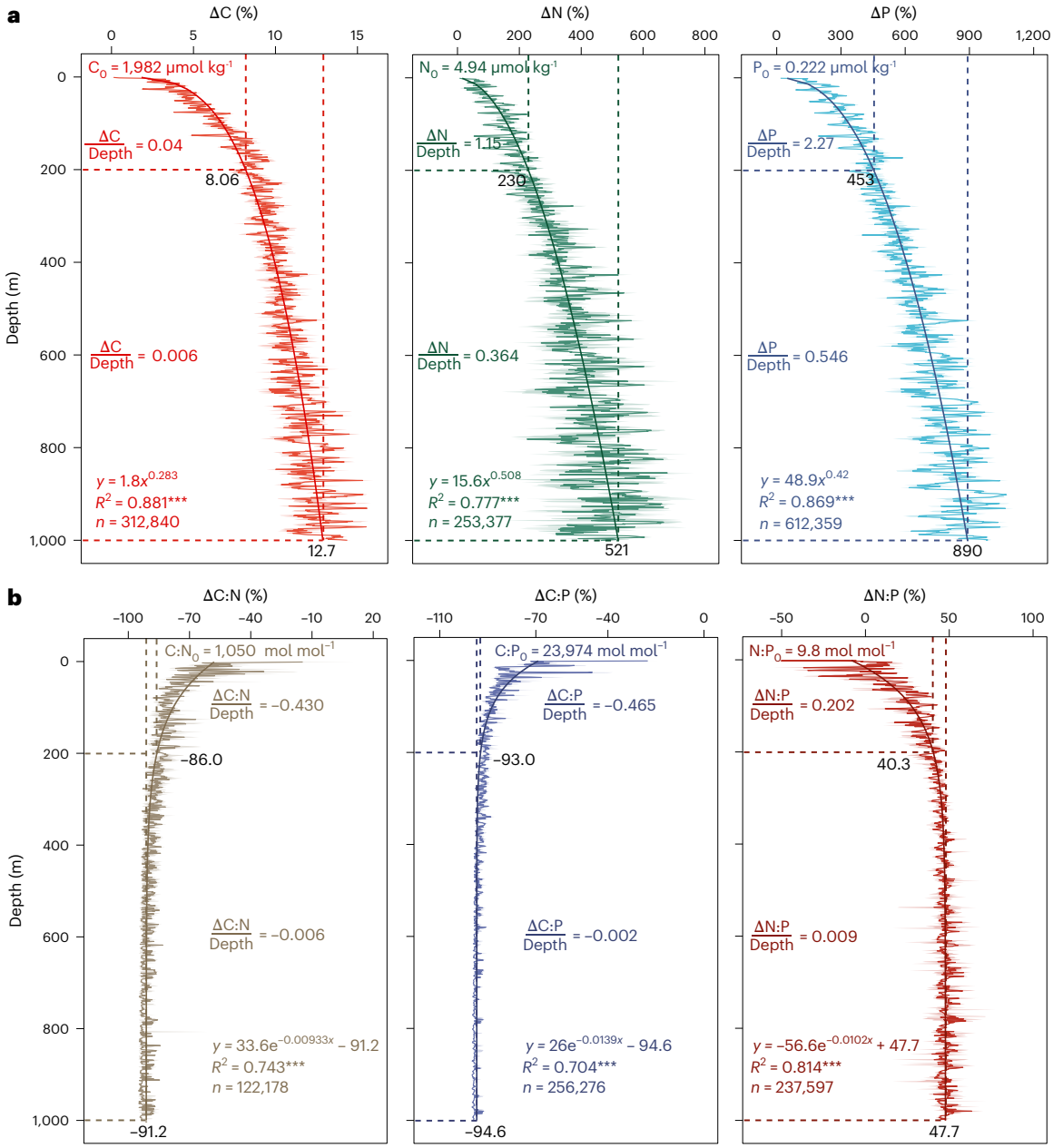

Fig. 3 | Depth-related changes in oceanic concentrations and stoichiometric ratios of C, N and P. a,**b**, Trends in the oceanic concentrations (**a**) and ecological stoichiometries (**b**) of C, N and P with different seawater depths. Δ represents the amount of change in the oceanic C, N and P concentrations at different seawater depths relative to that of the surface water. Predictor variables (C, N and P) plus lowercase 0 represent the mean value of the predictor variable at the seawater surface. Predictor variables (C:N, C:P, N:P) plus lowercase 0 represent the median value of the predictor variable at the seawater surface. The solid lines and shading area represent the mean for ΔC, ΔN and ΔP or median for ΔC:N, ΔC:P, and ΔN:P and 95% confidence intervals of the predictor variables, respectively. Predictor variables divided by depth represent the change coefficient of the predictor variables with increasing seawater depth in the epipelagic and mesopelagic zones. ***$P < 0.001$.

and trophic interactions, plankton effectively manage their C:N ratio in C-enriched marine environments[15]. These processes involve the transformation of CO_2 and N into fixed proportions of organic C and N, reflecting the plankton's inherent stoichiometric ratio[1]. The organic C and N synthesized in plankton biomass are subsequently released through growth and decay cycles, maintaining the overall C:N ratio in the marine ecosystem in a stable state[15]. Also, a recent global model with phytoplankton physiology suggests that planktonic C:N ratio is largely controlled by phytoplankton's physiological acclimation to environment especially the NO_3^- concentration and light intensity[43], as well as temperature[45], as these factors affect the ratio of N-rich protein to C in the cell[37,45,46]. The stability of the planktonic C:N ratio may indicate relative stability in these factors, or changes in these factors cancelling each other at the observed locations.

Uncertainties

Despite the robustness of our findings, several limitations should be acknowledged. First, the resolution of global marine C:N:P ratios is constrained by uneven sampling coverage, especially in mesopelagic zones at high latitudes. This spatial bias may underrepresent certain regional or seasonal variations in stoichiometry[47,48]. Second, our large-scale analysis may overlook microscale ecological

https://doi.org/10.1038/s41561-025-01735-y

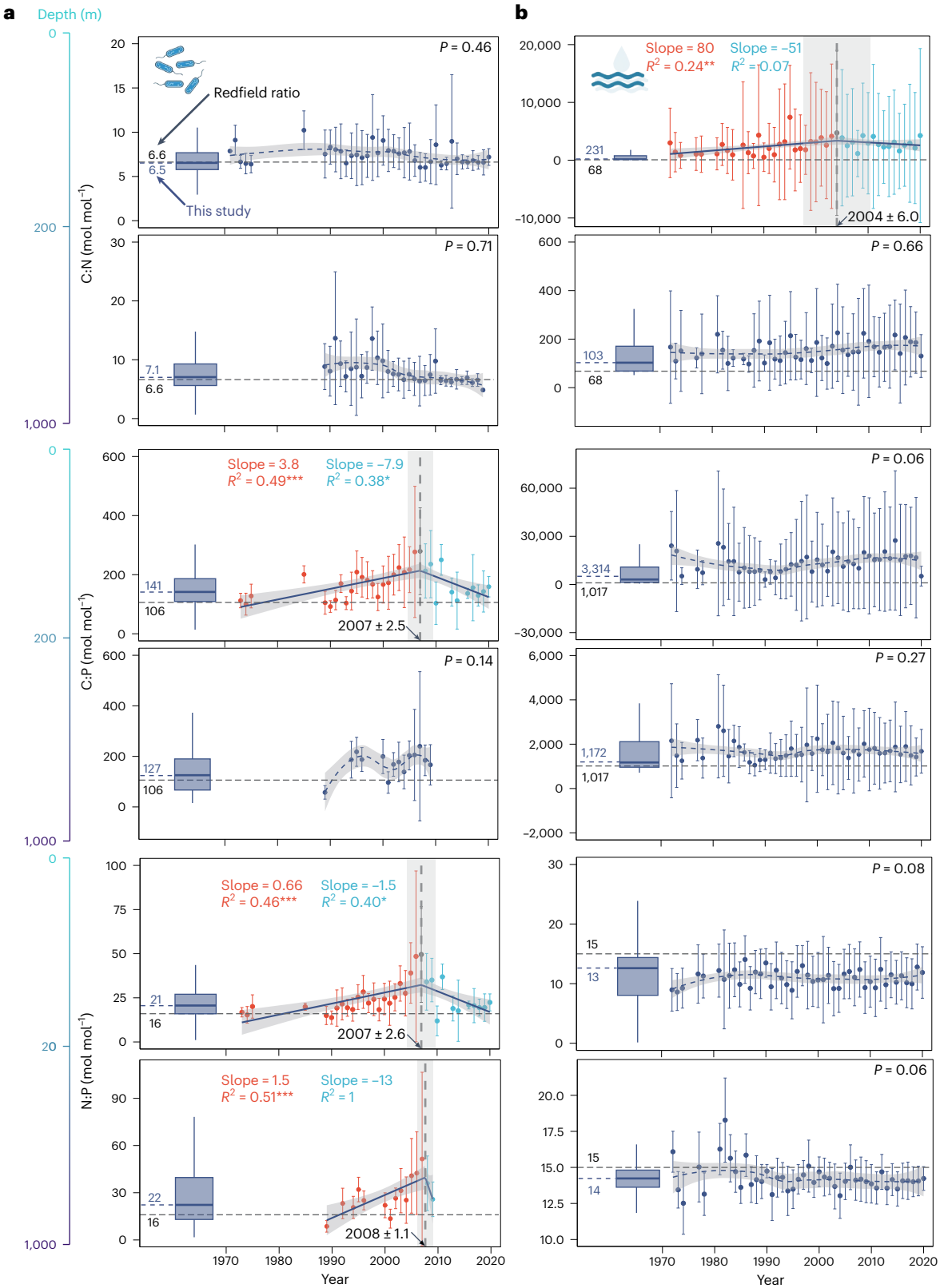

Fig. 4 | Temporal variation in marine ecological stoichiometric ratios over the past five decades. a,**b**, Temporal trends in planktonic (**a**, $n = 56{,}031$, particulate) and oceanic (**b**, $n = 388{,}515$, dissolved) ecological stoichiometry. The boxplot represents the distribution of data for all years from 1970 to 2020. For the boxplot, the straight line in the centre represents the median, or second quartile (Q2), the top edge of the box represents the third quartile (Q3) and the bottom edge of the box represents the first quartile (Q1). The dashed black and blue lines represent the Redfield ratio and the ecological stoichiometric ratio established in this study, respectively. The error bars represent the mean and standard deviation of the stoichiometric ratios for each year. The significance of the non-zero coefficients in the segmented model fitting is evaluated through a two-tailed *t*-test. If $P > 0.05$, it indicates that there is no obvious trend of change in the stoichiometric ratio over time. The shaded area of the fitted line represents the 95% confidence interval of the predicted values. The shaded area at the segmentation point represents the uncertainty of the time breakpoints, which is derived from the standard deviation of the breakpoint estimates across iterations based on resampling. $^{*}P < 0.05$, $^{**}P < 0.01$, $^{***}P < 0.001$.

https://doi.org/10.1038/s41561-025-01735-y

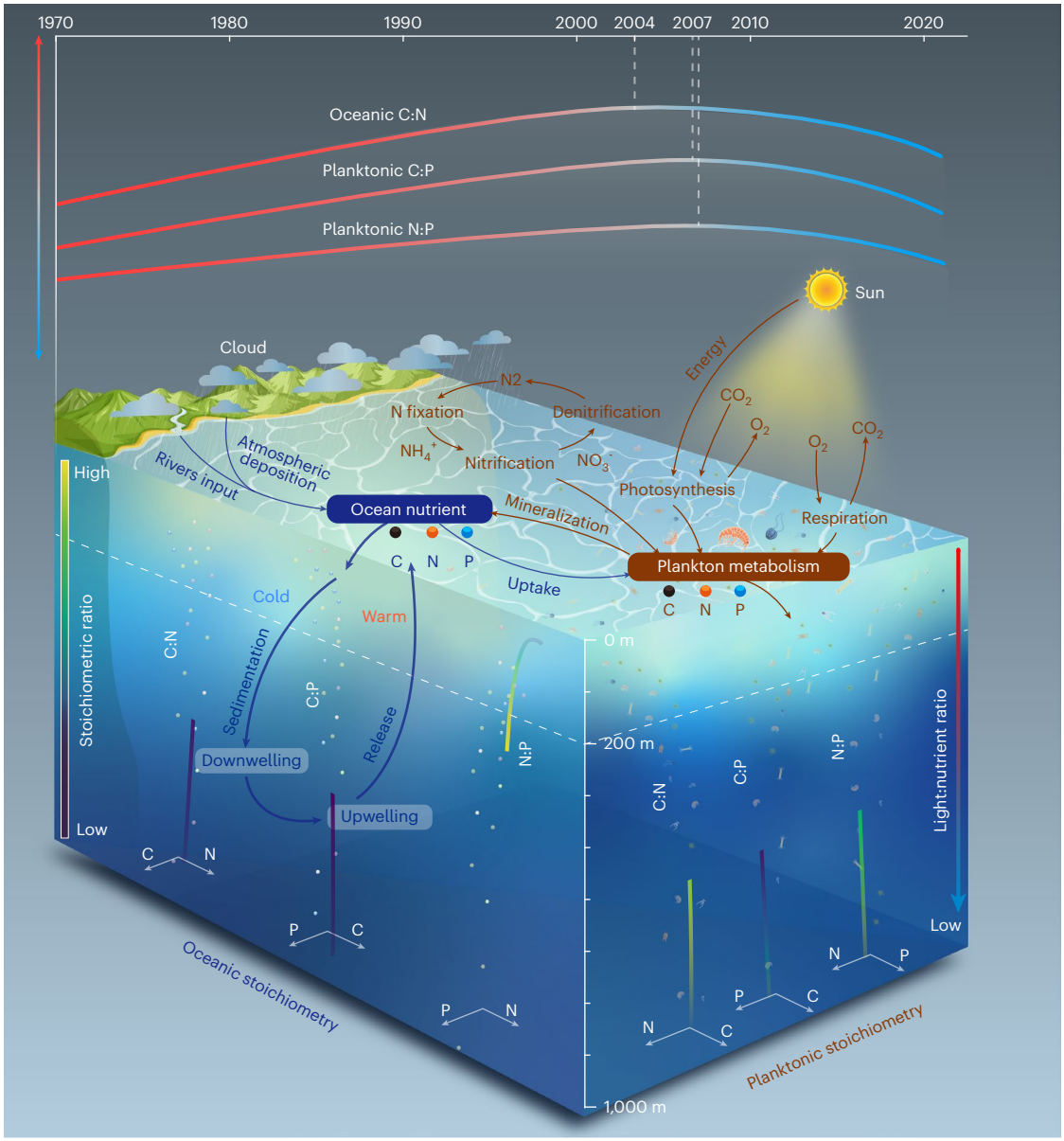

Fig. 5 | A conceptual diagram illustrating the spatiotemporal variations of marine ecological stoichiometries of C, N and P. This figure illustrates the conceptual framework of spatiotemporal dynamics in marine ecological stoichiometry for C, N and P, highlighting how their ratios and distributions vary across spatial scales and over time. The curves showing stoichiometric ratio changes with ocean depth are adapted from Fig. 3, while those reflecting temporal variations are based on Fig. 4.

processes—such as algal blooms, pollution events or community composition shifts—that significantly impact local elemental ratios[49]. Third, although we assessed long-term patterns, the potential influence of instrumental changes remains a concern. For instance, the Hawaii Ocean Time-series (HOT) reported a notable shift in planktonic P measurements after a 2011 equipment update[50,51]. However, sensitivity tests excluding HOT and Bermuda Atlantic Time-series Study (BATS) data still reproduced consistent C:P and N:P trends, supporting the overall robustness of our results. Lastly, the drivers of stoichiometric shifts remain complex. While our analyses emphasize pCO_2, nutrient inputs and stratification, other variables—such as temperature, iron and bioactive metals—also play significant roles but are difficult to quantify due to limited historical data[14,15,43,52]. Future studies should incorporate datasets such as GEOTRACES to explore the influence of trace metals on particle stoichiometry more comprehensively[53].

Conclusions

Our study reveals substantial global deviations from the classical Redfield ratios, with marine C:N:P stoichiometry varying markedly across depth and time (Fig. 5). These findings underscore the dynamic, non-static nature of marine elemental ratios, emphasizing the need for next-generation biogeochemical models that incorporate spatial heterogeneity, flexible stoichiometry and temporal feedbacks. Understanding such variability is crucial for predicting how marine ecosystems will respond to accelerating global change.

Online content

Any methods, additional references, Nature Portfolio reporting summaries, source data, extended data, supplementary information, acknowledgements, peer review information; details of author contributions and competing interests; and statements of data and code availability are available at https://doi.org/10.1038/s41561-025-01735-y.

References

1. Sterner, R. W. & Elser, J. J. *Ecological Stoichiometry: The Biology of Elements from Molecules to the Biosphere* (Princeton Univ. Press, 2002).
2. Redfield, A. C. The influence of organisms on the composition of seawater. *Sea* **2**, 26–77 (1963).
3. Penuelas, J. et al. Human-induced nitrogen-phosphorus imbalances alter natural and managed ecosystems across the globe. *Nat. Commun.* **4**, 2934 (2013).
4. Elser, J. et al. Nutritional constraints in terrestrial and freshwater food webs. *Nature* **408**, 578–580 (2000).
5. Redfield, A. C. in *James Johnstone Memorial Volume* (ed. Daniel, R. J.) 176–192 (Univ. Press Liverpool, 1934).
6. Gruber, N. & Deutsch, C. Redfield's evolving legacy. *Nat. Geosci.* **7**, 853–855 (2014).
7. Lipizer, M., Cossarini, G., Falconi, C., Solidoro, C. & Umani, S. F. Impact of different forcing factors on N:P balance in a semi-enclosed bay: the Gulf of Trieste (North Adriatic Sea). *Cont. Shelf Res.* **31**, 1651–1662 (2011).
8. Redfield, A. C. The biological control of chemical factors in the environment. *Am. Sci.* **46**, 205–221 (1958).
9. Martiny, A. C. et al. Strong latitudinal patterns in the elemental ratios of marine plankton and organic matter. *Nat. Geosci.* **6**, 279–283 (2013).
10. Falkowski, P. Rationalizing elemental ratios in unicellular algae. *J. Phycol.* **36**, 3–6 (2000).
11. Gerace, S. et al. Depth variance of organic matter respiration stoichiometry in the subtropical north atlantic and the implications for the global oxygen cycle. *Glob. Biogeochem. Cycles* **37**, e2023GB007814 (2023).
12. Gerace, S. D. et al. Observed declines in upper ocean phosphate-to-nitrate availability. *Proc. Natl Acad. Sci. USA* **122**, e2411835122 (2025).
13. Sterner, R., Elser, J. J., Fee, E., Guildford, S. J. & Chrzanowski, T. H. The light:nutrient ratio in lakes: the balance of energy and materials affects ecosystem structure and process. *Am. Nat.* **150**, 663–684 (1998).
14. Hutchins, D. & Capone, D. The marine nitrogen cycle: new developments and global change. *Nat. Rev. Microbiol.* **20**, 401–414 (2022).
15. Gruber, N. Consistent patterns of nitrogen fixation identified in the ocean. *Nature* **566**, 191–193 (2019).
16. Moreno, A., Hagstrom, G., Primeau, F., Levin, S. & Martiny, A. Marine phytoplankton stoichiometry mediates nonlinear interactions between nutrient supply, temperature, and atmospheric CO_2. *Biogeosciences* **15**, 2761–2779 (2018).
17. Pan, Y. et al. Enhanced atmospheric phosphorus deposition in Asia and Europe in the past two decades. *Atmos. Ocean. Sci. Lett.* **14**, 100051 (2021).
18. Ackerman, D., Millet, D. B. & Chen, X. Global estimates of inorganic nitrogen deposition across four decades. *Glob. Biogeochem. Cycles* **33**, 100–107 (2019).
19. Friedlingstein, P. et al. Global carbon budget 2022. *Earth Syst. Sci. Data* **14**, 4811–4900 (2022).
20. van de Waal, D. B., Verschoor, A. M., Verspagen, J. M. H., van Donk, E. & Huisman, J. Climate-driven changes in the ecological stoichiometry of aquatic ecosystems. *Front. Ecol. Environ.* **8**, 145–152 (2010).
21. Hutchins, D., Mulholland, M. & Feixue, F. Nutrient cycles and marine microbes in a CO_2-enriched ocean. *Oceanography* **22**, 128–145 (2009).
22. Guignard, M. et al. Impacts of nitrogen and phosphorus: from genomes to natural ecosystems and agriculture. *Front. Ecol. Evol.* https://doi.org/10.3389/fevo.2017.00070 (2017).
23. Ayo, B. et al. Imbalanced nutrient recycling in a warmer ocean driven by differential response of extracellular enzymatic activities. *Glob. Chang. Biol.* **23**, 4084–4093 (2017).
24. Toseland, A. et al. The impact of temperature on marine phytoplankton resource allocation and metabolism. *Nat. Clim. Chang.* **3**, 979–984 (2013).
25. Alewell, C. et al. Global phosphorus shortage will be aggravated by soil erosion. *Nat. Commun.* **11**, 4546 (2020).
26. Matsumoto, K., Tanioka, T. & Rickaby, R. Linkages between dynamic phytoplankton C:N:P and the ocean carbon cycle under climate change. *Oceanography* **33**, 44–52 (2020).
27. Tanaka, T. et al. Availability of phosphate for phytoplankton and bacteria and of glucose for bacteria at different pCO_2 levels in a mesocosm study. *Biogeosciences* **5**, 669–678 (2008).
28. Paul, C., Matthiessen, B. & Sommer, U. Warming, but not enhanced CO_2 concentration, quantitatively and qualitatively affects phytoplankton biomass. *Mar. Ecol. Prog. Ser.* **528**, 39–51 (2015).
29. Bellerby, R. et al. Marine ecosystem community carbon an nutrient uptake stoichiometry under varying ocean acidification during the PeECE III experiment. *Biogeosciences* **5**, 1517–1527 (2008).
30. Deutsch, C. & Weber, T. Nutrient ratios as a tracer and driver of ocean biogeochemistry. *Ann. Rev. Mar. Sci.* **4**, 113–141 (2012).
31. Islam, M. et al. C:N:P stoichiometry of particulate and dissolved organic matter in river waters and changes during decomposition. *J. Ecol. Environ.* **43**, 4 (2019).
32. Louis, J., Bressac, M., Pedrotti, M. L. & Guieu, C. Dissolved inorganic nitrogen and phosphorus dynamics in seawater following an artificial Saharan dust deposition event. *Front. Mar. Sci.* **2**, 27 (2015).
33. Ward, B. B. et al. Denitrification as the dominant nitrogen loss process in the Arabian Sea. *Nature* **461**, 78–81 (2009).
34. Fakhraee, M., Planavsky, N. & Reinhard, C. The role of environmental factors in the long-term evolution of the marine biological pump. *Nat. Geosci.* **13**, 812–816 (2020).
35. Tanioka, T. & Matsumoto, K. A meta-analysis on environmental drivers of marine phytoplankton C:N:P. *Biogeosciences* **17**, 2939–2954 (2020).
36. Weber, T., Deutsch, C., Weber, T. S. & Deutsch, C. Ocean nutrient ratios governed by plankton biogeography. *Nature* **467**, 550–554 (2010).
37. Liefer, J. et al. The macromolecular basis of phytoplankton C:N:P under nitrogen starvation. *Front. Microbiol.* **10**, 763 (2019).
38. Guo, L. et al. Acceleration of phosphorus weathering under warm climates. *Sci. Adv.* **10**, eadm7773 (2024).
39. Seitzinger, S. P. et al. Global river nutrient export: a scenario analysis of past and future trends. *Glob. Biogeochem. Cycles* **24**, GB0A08 (2010).
40. Lapointe, B. E. et al. Nutrient content and stoichiometry of pelagic *Sargassum* reflects increasing nitrogen availability in the Atlantic Basin. *Nat. Commun.* **12**, 3060 (2021).
41. Wang, M. et al. The great Atlantic Sargassum belt. *Science* **365**, 83–87 (2019).
42. Kwiatkowski, L., Aumont, O., Bopp, L. & Ciais, P. The impact of variable phytoplankton stoichiometry on projections of primary production, food quality, and carbon uptake in the global ocean. *Glob. Biogeochem. Cycles* **32**, 516–528 (2018).
43. Inomura, K., Deutsch, C., Jahn, O., Dutkiewicz, S. & Follows, M. Global patterns in marine organic matter stoichiometry driven by phytoplankton ecophysiology. *Nat. Geosci.* **15**, 1034–1040 (2022).
44. Moore, C. et al. Processes and patterns of oceanic nutrient limitation. *Nat. Geosci.* **6**, 701–710 (2013).
45. Armin, G. & Inomura, K. Modeled temperature dependencies of macromolecular allocation and elemental stoichiometry in phytoplankton. *Comput. Struct. Biotechnol. J.* **19**, 5421–5427 (2021).

46. Liefer, J. et al. Latitudinal patterns in ocean C:N:P reflect phytoplankton acclimation and macromolecular composition. *Proc. Natl Acad. Sci. USA* **121**, e2404460121 (2024).
47. Sterner, R. W. et al. Scale-dependent carbon:nitrogen:phosphorus seston stoichiometry in marine and freshwaters. *Limnol. Oceanogr.* **53**, 1169–1180 (2008).
48. Frigstad, H. et al. Seasonal variation in marine C:N:P stoichiometry: can the composition of seston explain stable Redfield ratios? *Biogeosciences* **8**, 2917–2933 (2011).
49. Berry, D. L. et al. Shifts in Cyanobacterial Strain Dominance during the Onset of Harmful Algal Blooms in Florida Bay, USA. *Microb. Ecol.* **70**, 361–371 (2015).
50. Martiny, A., Vrugt, J. & Lomas, M. Concentrations and ratios of particulate organic carbon, nitrogen, and phosphorus in the global ocean. *Sci. Data* **1**, 140048 (2014).
51. Tanioka, T. et al. Global patterns and predictors of C:N:P in marine ecosystems. *Commun. Earth Environ.* **3**, 271 (2022).
52. Hutchins, D. A. & Tagliabue, A. Feedbacks between phytoplankton and nutrient cycles in a warming ocean. *Nat. Geosci.* **17**, 495–502 (2024).
53. Conway, T. M., Horner, T. J., Plancherel, Y. & González, A. G. A decade of progress in understanding cycles of trace elements and their isotopes in the oceans. *Chem. Geol.* **580**, 120381 (2021).

Publisher's note Springer Nature remains neutral with regard to jurisdictional claims in published maps and institutional affiliations.

Springer Nature or its licensor (e.g. a society or other partner) holds exclusive rights to this article under a publishing agreement with the author(s) or other rightsholder(s); author self-archiving of the accepted manuscript version of this article is solely governed by the terms of such publishing agreement and applicable law.

© The Author(s), under exclusive licence to Springer Nature Limited 2025

[1]State Key Laboratory of Loess Science, Institute of Earth Environment, Chinese Ac ademy of Sciences, Xi'an, China. [2]Hubei Province Key Laboratory for Geographical Process Analysis and Simulation, Central China Normal University, Wuhan, China. [3]CSIC, Global Ecology Unit CREAF-CSIC-UAB, Bellaterra, Spain. [4]CREAF, Bellaterra, Spain. [5]Laboratorio de Biodiversidad y Funcionamiento Ecosistémico, Instituto de Recursos Naturales y Agrobiología de Sevilla, Consejo Superior de Investigaciones Científicas, Seville, Spain. [6]Department of Earth System Science, University of California, Irvine, Irvine, CA, USA. [7]Marine and Environmental Biology, University of Southern California, Los Angeles, CA, USA. [8]Graduate School of Oceanography, University of Rhode Island, Narragansett, RI, USA. [9]Bigelow Laboratory for Ocean Sciences, East Boothbay, ME, USA. [10]Department of Earth and Planetary Sciences, Yale University, New Haven, CT, USA. [11]Department of Plant Sciences, University of Cambridge, Cambridge, UK. [12]Department of Ecology, Faculty of Science, Charles University, Prague, Czechia. [13]Department of Geosciences, and at the High Meadows Environmental Institute, Princeton University, Princeton, NJ, USA. [14]Harbor Branch Oceanographic Institute, Florida Atlantic University, Ft. Pierce, FL, USA. [15]Ministry of Education Key Laboratory for Transboundary Ecosecurity of Southwest China, School of Ecology and Environmental Science, Yunnan University, Kunming, China. [16]Key Laboratory of Agro-ecological Processes in Subtropical Regions, Institute of Subtropical Agriculture, Chinese Academy of Sciences, Changsha, China. [17]Institute of Atmospheric Physics, Chinese Academy of Sciences, Beijing, China. [18]Institute of Global Environmental Change, Department of Earth and Environmental Science, School of Human Settlements and Civil Engineering, Xi'an Jiaotong University, Xi'an, China. [19]Guanzhong Plain Ecological Environment Change and Comprehensive Treatment National Observation and Research Station, Xi'an, China. ✉e-mail: chenji@ieecas.cn

Methods

Planktonic and oceanic ecological stoichiometries

We integrated data encompassing samples of plankton (n = 56,031) and ocean (n = 388,515) from depths ranging from 0 to 1,000 m to determine variations in marine ecological stoichiometry[50,51,54,55] (Fig. 1 and Supplementary Table 1). The calculation of planktonic ecological stoichiometry used particulate organic carbon, particulate organic nitrogen and particulate organic phosphorus as indicators. Due to the difficulty in distinguishing living from dead plankton in practical applications, the ecological stoichiometry of plankton is referred to as 'particulate state' without further differentiation. For oceanic ecological stoichiometry, dissolved inorganic carbon, dissolved inorganic nitrate plus nitrite, and dissolved inorganic phosphate were utilized. These measurements follow globally standard protocols, where seawater particles are collected on glass fibre filters (Whatman GF/F, nominal 0.7 µm pore size) and analysed using a combustion gas chromatography–infrared spectroscopy elemental analyser[50].

Adopting Redfield's statistical framework, we calculated planktonic and oceanic ecological stoichiometry ratio using median values of C:N:P, while biological activity ratio was derived from the slopes of least-squares fitted equations correlating C, N and P molar concentrations[2] (Fig. 2). Notably, Redfield did not specify the intercepts for these fitting equations; therefore, in our analysis, we used the slope of the best-fit least-squares equation to ascertain the biological activity ratio. Biological activity refers to the dynamic regulation of oceanic chemical composition through marine organisms' life processes (for example, nutrient assimilation, metabolic excretion and organic matter decomposition).

Considering the huge volume and high degree of overlap of planktonic and oceanic samples, to visualize the distribution of C:N:P ratio across the epipelagic (0–200 m) and mesopelagic (201–1,000 m) zones, we used the R package 'Hexbin' to present the distribution patterns of the samples in the form of density maps. We divided the concentration range of oceanic C, N and P concentration into 50 × 50 hexagonal cells, with each hexagon representing a specific region. The density of these regions is reflected by the number of data points within each hexagon. The calculation formula is

$$\text{Density} = \frac{\text{Count}_i}{\text{Total}}, \tag{1}$$

where Count_i represents the number of sample points within the concentration range of the ith hexagonal cell and Total represents the total number of sample points. By observing the colour variations across different regions, one can intuitively understand the distribution characteristics of C, N and P concentration combinations and identify hotspots or sparse areas within the dataset.

To assess whether the Redfield ratio significantly differs from the ecological stoichiometric ratio established in this study, we computed confidence intervals for the medians to evaluate the variability of marine ecological stoichiometry relative to the Redfield ratio. We used a non-parametric approach[56] to estimate the confidence interval for the population median, using the following formulas (Table 1, Extended Data Table 1 and Supplementary Fig. 3):

$$j = nq - z\sqrt{nq(1-q)} \tag{2}$$

$$j = nq + z\sqrt{nq(1-q)}, \tag{3}$$

where n represents the sample size, q represents the quantile of interest and z represents the critical value. For the median, we use q = 0.5. For a 95% confidence level, we use z = 1.96. j and k represent the positions of the lower and upper bounds of the confidence interval. We round j and k up to integer. The resulting confidence interval lies between the jth and kth observations in the ordered sample data.

For the P values of differences between current stoichiometric ratio (1970–2020) and Redfield ratio, we used the Wilcoxon rank-sum test (also known as the Mann–Whitney U test)[57,58] (Table 1, Extended Data Table 1 and Supplementary Fig. 3). Observations from both groups (group A and group B) were combined and sorted in ascending order. Each observation was assigned a rank. In the case of ties (that is, identical values), the average rank was assigned. The sum of ranks was calculated separately for each group, denoted as R_1 (group A) and R_2 (group B). The test statistic U was computed on the basis of the rank sums using

$$U = n_1 n_2 + \frac{n_1(n_1+1)}{2} - R_1, \tag{4}$$

where n_1 and n_2 are the sample sizes of the two groups, and R_1 is the rank sum of group A. The P value was derived from the U statistic and sample sizes, either by referencing a statistical table (for small samples) or using a normal approximation (for large samples). The P value represents the probability of observing the calculated U (or a more extreme value) under the null hypothesis that the medians of the two groups are equal. The test was implemented using the Wilcox.test function in R. This method is advantageous as it does not require the assumption of normality and is robust to outliers, making it suitable for non-parametric comparisons.

Due to the significant variation in ecological stoichiometric ratio observed in the epipelagic zone, we further calculated the median values of these ratios at 10-m intervals from 0 m to 100 m to better understand the changes at these depths. We also used Dunn's Kruskal–Wallis method to assess the significant variability of oceanic ecological stoichiometry ratio across different water depths (Supplementary Fig. 4).

Vertical trends in oceanic ecological stoichiometry

In our analyses, we observed notable depth variability in the oceanic ecological stoichiometry, while such variability was less pronounced in planktonic ecological stoichiometry (Fig. 3 and Extended Data Fig. 2). To explore these depth-dependent variations in the molar concentrations and ratios of C, N and P, we applied a power function and exponential function to model the trends in oceanic ecological stoichiometry as a function of depth. The relative changes (Δ) in the concentrations and ratios of C, N and P with increasing depth were calculated using

$$\Delta C\,(\Delta N;\Delta P) = \frac{C\,(N;P) - C_0\,(N_0;P_0)}{C_0\,(N_0;P_0)} \times 100 \tag{5}$$

$$\Delta C : N\,(\Delta C : P;\Delta N : P) = \frac{C : N(C : P;N : P) - C : N_0\,(C : P_0;N : P_0)}{C : N_0\,(C : P_0;N : P_0)} \times 100, \tag{6}$$

where C, N and P denote the oceanic concentrations of carbon, nitrogen and phosphorus (µmol kg^{-1}), respectively, and C_0, N_0 and P_0 represent the concentrations of C, N and P in the surface seawater (0 m), respectively. C:N, C:P and N:P denote the oceanic molar ratio of carbon, nitrogen and phosphorus (mol mol^{-1}), and C:N_0, C:P_0 and N:P_0 represent the molar ratio of C:N, C:P and N:P in the surface seawater (0 m), respectively. The baseline values are C_0 = 1,982 ± 71 (µmol kg^{-1}; mean ± s.d.), N_0 = 4.94 ± 6.43 (µmol kg^{-1}; mean ± s.d.), P_0 = 0.222 ± 0.374 (µmol kg^{-1}; mean ± s.d.), C:N_0 = 1,050 ± 1,391 (mol mol^{-1}; median ± median absolute deviation (MAD), C:P_0 = 23,974 ± 30,720 (mol mol^{-1}; median ± MAD), N:P_0 = 9.8 ± 4.83 (mol mol^{-1}; median ± MAD). The s.d. is the square root of the average degree of deviation of data from the mean, reflecting the volatility of data around the mean. The MAD is the median of the absolute deviations of data from the median, reflecting the volatility of data around the median.

$$\text{MAD} = \text{median}\left(|x_i - \text{median}|\right), \tag{7}$$

where x_i represents the ith observation in the dataset. We utilized the 'plot3D' package to visualize the vertical variability of oceanic and planktonic C, N and P concentrations and their stoichiometric ratios across the 0–1,000 m depth gradient (Fig. 3 and Supplementary

Fig. 5). Incorporating key biogeochemical processes into the analysis of marine ecological stoichiometry enables a spatially explicit understanding of how these processes drive stoichiometric heterogeneity.

Temporal trends in the planktonic and oceanic ecological stoichiometries

We analysed the ecological stoichiometric ratio of C, N and P across 11 global marine regions within a calendar year, utilizing area-weighted averages to assess global marine ecological stoichiometry. This methodology helps to mitigate the uncertainty in global assessments caused by sampling biases, which may occur due to the concentration of sampling efforts in a limited number of regions during certain years. To address this, we partitioned the global seas into several areas based on classifications provided by the International Hydrographic Organization and the Flanders Marine Institute. These areas include the Arctic Ocean, the North and South Atlantic Oceans, the North and South Pacific Oceans, the Southern Ocean, the Indian Ocean, the Baltic Sea, the Mediterranean Region, and the South China and Eastern Archipelagic Seas (source: https://www.marineregions.org/) (Supplementary Fig. 1).

Weighted averages were used to calculate the global stoichiometric ratio, factoring in the total oceanic area represented by these regions. The calculations were conducted using

$$\bar{X} = \sum_{i=1}^{n}\left(\bar{X}_i \times \frac{\mathrm{Area}_i}{\sum_{j=1}^{n}\mathrm{Area}_j}\right) \tag{8}$$

$$\mathrm{Var}\,(X) = \sum_{i=1}^{n}\left(\mathrm{Var}\,(X_i) \times \frac{\mathrm{Area}_i}{\sum_{j=1}^{n}\mathrm{Area}_j}\right), \tag{9}$$

where $\bar{X}$ represents the mean stoichiometric ratio, Var(X) represents the variance of the stoichiometric ratio, (i,j) represents the sea area where samples were collected, n represents the number of sea areas covered by all sampling points in a year, and we mark the sea areas as (1, 2, 3… n) (Fig. 1).

To assess changes in marine ecological stoichiometry from 1971 to 2020, we utilized the 'segmented' package in R (ref. 59). This analysis identified breakpoints in linear fits, serving as threshold years that indicate potential shifts in marine ecological stoichiometry (Fig. 4, Extended Data Figs. 3–6 and Supplementary Figs. 6–14). The 95% confidence intervals for the fitted lines and breakpoints were calculated and visualized as shaded areas. In cases where relationships between variables were not statistically significant, visual smoothing was applied using the loess function to elucidate underlying patterns.

Furthermore, boxplots were incorporated into temporal trend plots to compare differences between planktonic and oceanic ecological stoichiometry relative to the Redfield ratio over the study period (Fig. 4). In these boxplots, the central line represents the median or second quartile, offering a robust measure of central tendency. The top and bottom edges of the box denote the third and first quartiles, representing the upper and lower 25% of the data, respectively. This graphical representation aids in illustrating the distribution and variability of ecological stoichiometry over time.

Data availability

The datasets generated and analysed during the current study are available via figshare at https://doi.org/10.6084/m9.figshare.27282792 (ref. 60).

References

54. Dietze, H., Oschlies, A. & Kähler, P. *Concentrations of Organic Carbon, Nitrogen and Phosphorus on Vertical Profiles in Waters of the Tropical North Atlantic in March 2002* (PANGAEA, 2008).
55. Lauvset, S. et al. An updated version of the global interior ocean biogeochemical data product, GLODAPv2.2021. *Earth Syst. Sci. Data* **13**, 5565–5589 (2021).
56. Conover, W. J. in *Practical Nonparametric Statistics* (ed. Wiley, B. II) Ch. 3 (Wiley & Sons, 1999).
57. Wilcoxon, F. Individual comparisons by ranking methods. *Biom. Bull.* **1**, 80–83 (1945).
58. Mann, H. B. & Whitney, D. R. On a test of whether one of two random variables is stochastically larger than the other. *Ann. Stat.* **18**, 50–60 (1947).
59. Toms, J. & Lesperance, M. Piecewise regression: a tool for identifying ecological thresholds. *Ecology* **84**, 2034–2041 (2003).
60. Liu, J. et al. Database title. *figshare* https://doi.org/10.6084/m9.figshare.27282792 (2025).
61. Reay, D. S., Dentener, F., Smith, P., Grace, J. & Feely, R. A. Global nitrogen deposition and carbon sinks. *Nat. Geosci.* **1**, 430–437 (2008).
62. Graber, J., Amthor, J., Dahlman, R., Drell, D. & Weatherwax, S. *Carbon Cycling and Biosequestration Integrating Biology and Climate Through Systems Science Report from the March 2008 Workshop* (US Department of Energy Office of Science, 2008).
63. Galloway, J. N. et al. Nitrogen cycles: past, present, and future. *Biogeochemistry* **70**, 153–226 (2004).
64. Zhang, X., Ward, B. B. & Sigman, D. M. Global nitrogen cycle: critical enzymes, organisms, and processes for nitrogen budgets and dynamics. *Chem. Rev.* **120**, 5308–5351 (2020).
65. Wang, R. et al. Significant contribution of combustion-related emissions to the atmospheric phosphorus budget. *Nat. Geosci.* **8**, 48–54 (2015).

Acknowledgements

J.L. is funded by the National Natural Science Foundation of China (grant no. 42207107) and the Horizon Europe Framework Programme (grant no. 101205485). K.I. is supported by a grant from the Simons Foundation (grant no. LS-ECIAMEE-00001549). Ji.C. is granted by the National Natural Science Foundation of China (grant nos. 32471685 and 42361144886) and Shaanxi Province Natural Science Foundation for Distinguished Young Scholar (grant no. 2024JC-JCQN-32).

Author contributions

J.L. conceived the study. J.L., H.W. and J.M. designed the methodology, conducted the investigation and generated the visualizations. J.L. drafted the paper. Ji.C. and J.P. supervised the project. J.L., H.W., J.M., J.P., M.D.-B., A.C.M., G.Z., D.A.H., K.I., M.W.L., M.F., A.P., T.J.K., C.A.D., N.P., B.L., Yo.Z., Ya.L., J.Z., Yi.Z., S.S., Yo.L., W.Z., Ju.C. and Ji.C. reviewed and edited the paper.

Competing interests

The authors declare no competing interests.

Additional information

Extended data is available for this paper at https://doi.org/10.1038/s41561-025-01735-y.

Supplementary information The online version contains supplementary material available at https://doi.org/10.1038/s41561-025-01735-y.

Correspondence and requests for materials should be addressed to Ji Chen.

Peer review information *Nature Geoscience* thanks Dag Hessen, Helena Klip and the other, anonymous, reviewer(s) for their contribution to the peer review of this work. Primary Handling Editor: James Super, in collaboration with the *Nature Geoscience* team.

Reprints and permissions information is available at www.nature.com/reprints.

https://doi.org/10.1038/s41561-025-01735-y

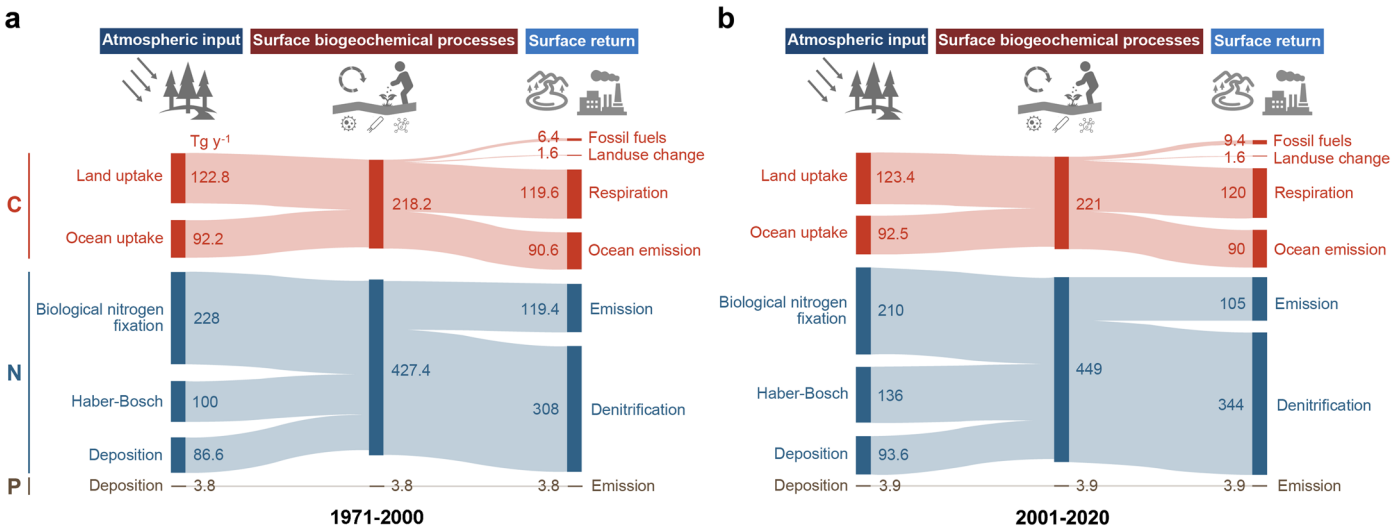

Extended Data Fig. 1 | Fluxes of carbon (C), nitrogen (N), and phosphorus (P) in atmospheric inputs to the surface versus surface returns to the atmosphere from 1971 to 2000 (a) and 2001 to 2020 (b). The data on the global C cycle are from Reay et al.[61], Graber et al.[62], and Friedlingstein et al.[19]. The data on the global N are from Galloway et al.[63], Zhang et al.[64], and Ackerman et al.[18]. The data on the global P cycle are from Wang et al.[65].

https://doi.org/10.1038/s41561-025-01735-y

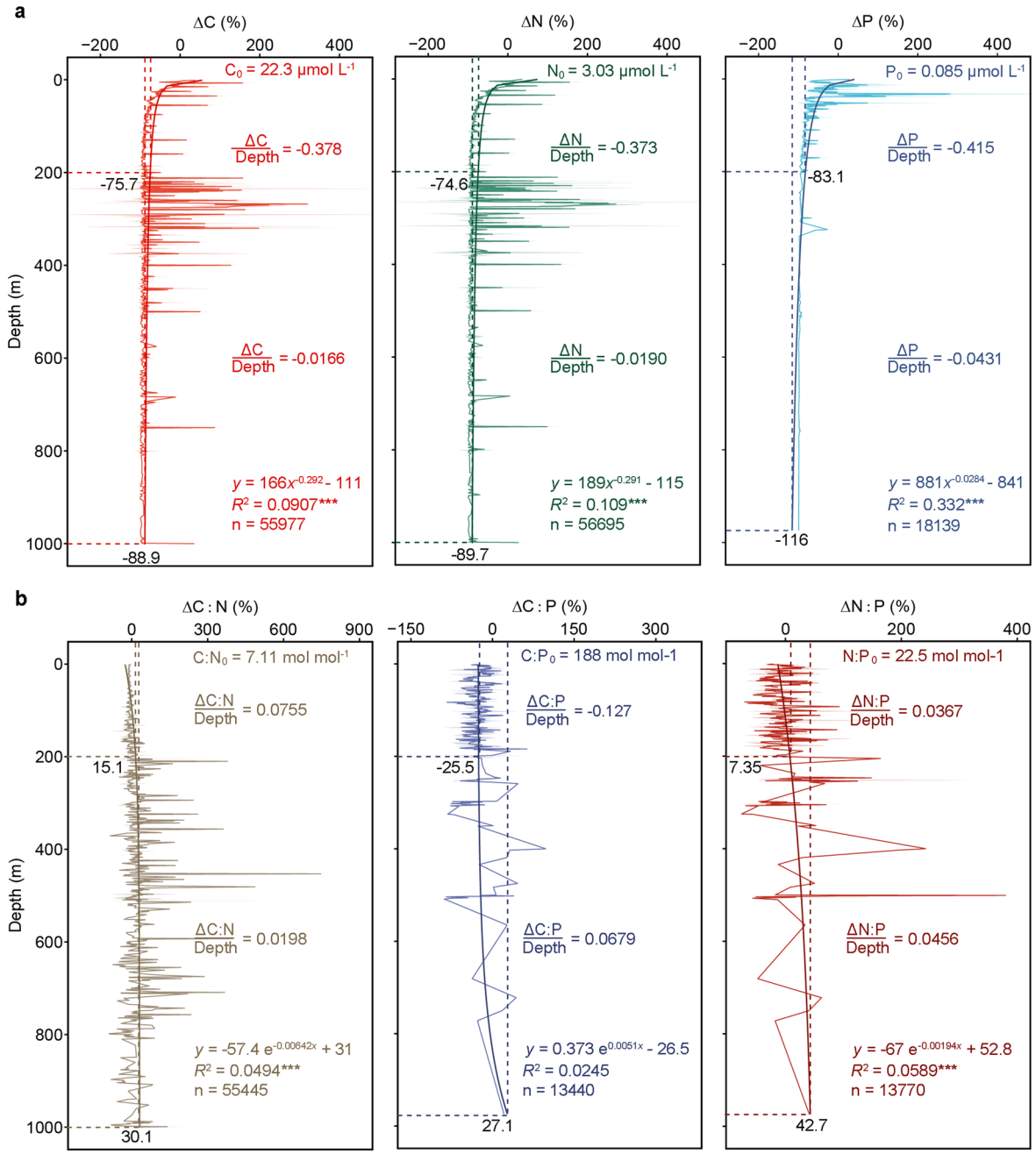

Extended Data Fig. 2 | Trends in the planktonic concentrations (a) and stoichiometries (b) of carbon (C), nitrogen (N) and phosphorus (P) at different seawater depths. Δ represents the amount of change in the planktonic C, N, and P concentrations at different seawater depths relative to that of the surface water. Predictor variables (C, N, P) plus lowercase 0 represent the mean value of the predictor variable at the seawater surface. Predictor variables (C:N, C:P, N:P) plus lowercase 0 represent the median value of the predictor variable at the seawater surface. The solid lines and shading area represent the mean for ΔC, ΔN, and ΔP or median for ΔC:N, ΔC:P, and ΔN:P and 95% confidence intervals of the predictor variables, respectively. Predictor variables divided by depth represent the change coefficient of the predictor variables with increasing seawater depth in the epipelagic and mesopelagic zones. ***, $p < 0.001$.

https://doi.org/10.1038/s41561-025-01735-y

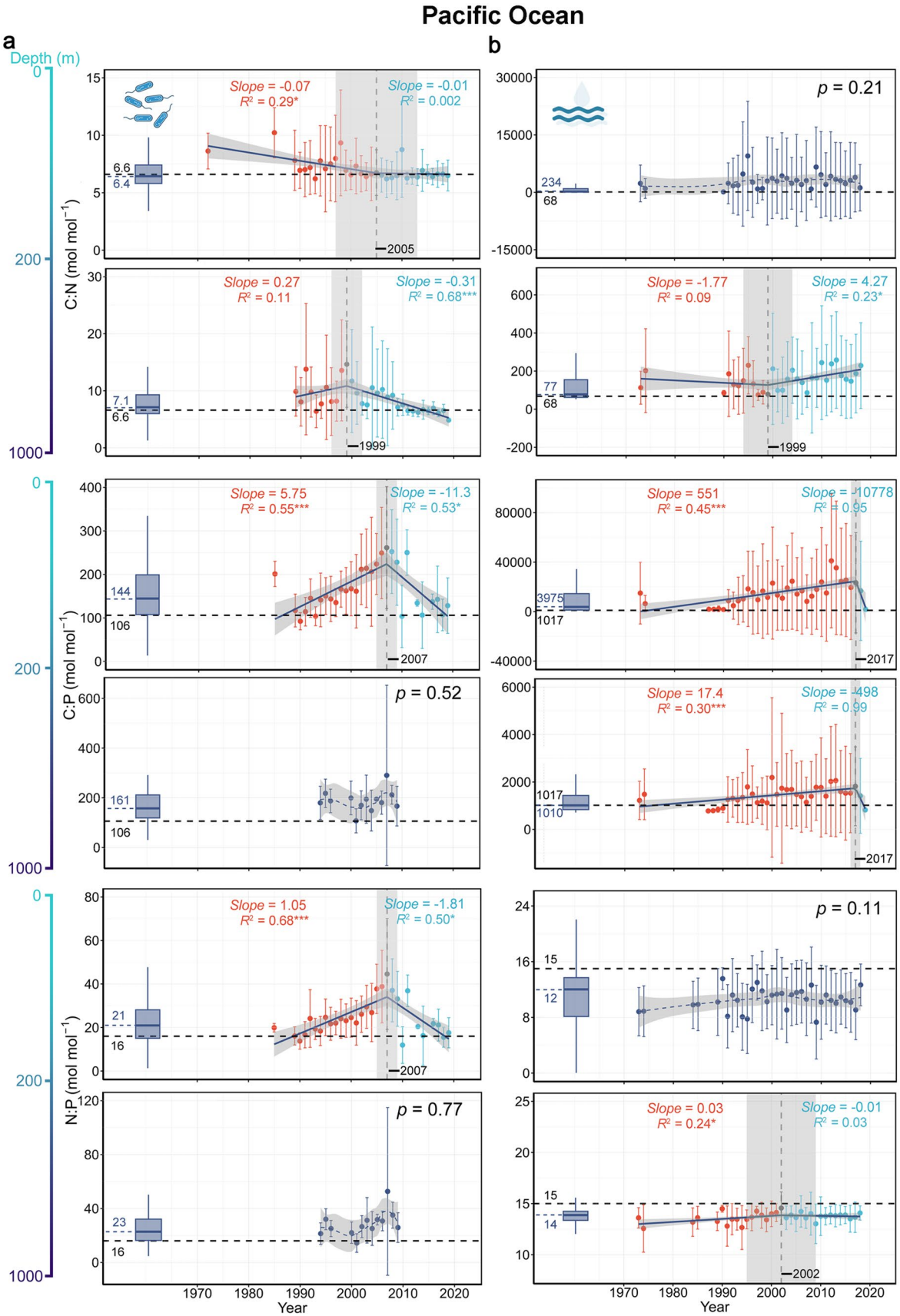

Extended Data Fig. 3 | See next page for caption.

https://doi.org/10.1038/s41561-025-01735-y

Extended Data Fig. 3 | Temporal trends in planktonic (a, n = 28135) and oceanic (b, n = 177487) ecological stoichiometry of the Pacific Ocean. The boxplot represents the distribution of data for all years from 1970 to 2020. For the boxplot, the straight line in the center represents the median, or 2nd quartile (Q2), the top edge of the box represents the 3rd quartile (Q3), and the bottom edge of the box represents the 1st quartile (Q1). The black and blue dashed lines represent the Redfield ratio and the ecological stoichiometric ratio established in this study, respectively. The error bars represent the mean and standard deviation of the stoichiometric ratios for each year. The significance of the non-zero coefficients in the segmented model fitting is evaluated through a two-tailed t-test. If $p > 0.05$, it indicates that there is no obvious trend of change in the stoichiometric ratio over time. The shaded area of the fitted line represents the 95% confidence interval of the predicted values. The shaded area at the segmentation point represents the uncertainty of the time breakpoints, which is derived from the standard deviation of the breakpoint estimates across iterations based on resampling. *, $p < 0.05$; **, $p < 0.01$; ***, $p < 0.001$.

https://doi.org/10.1038/s41561-025-01735-y

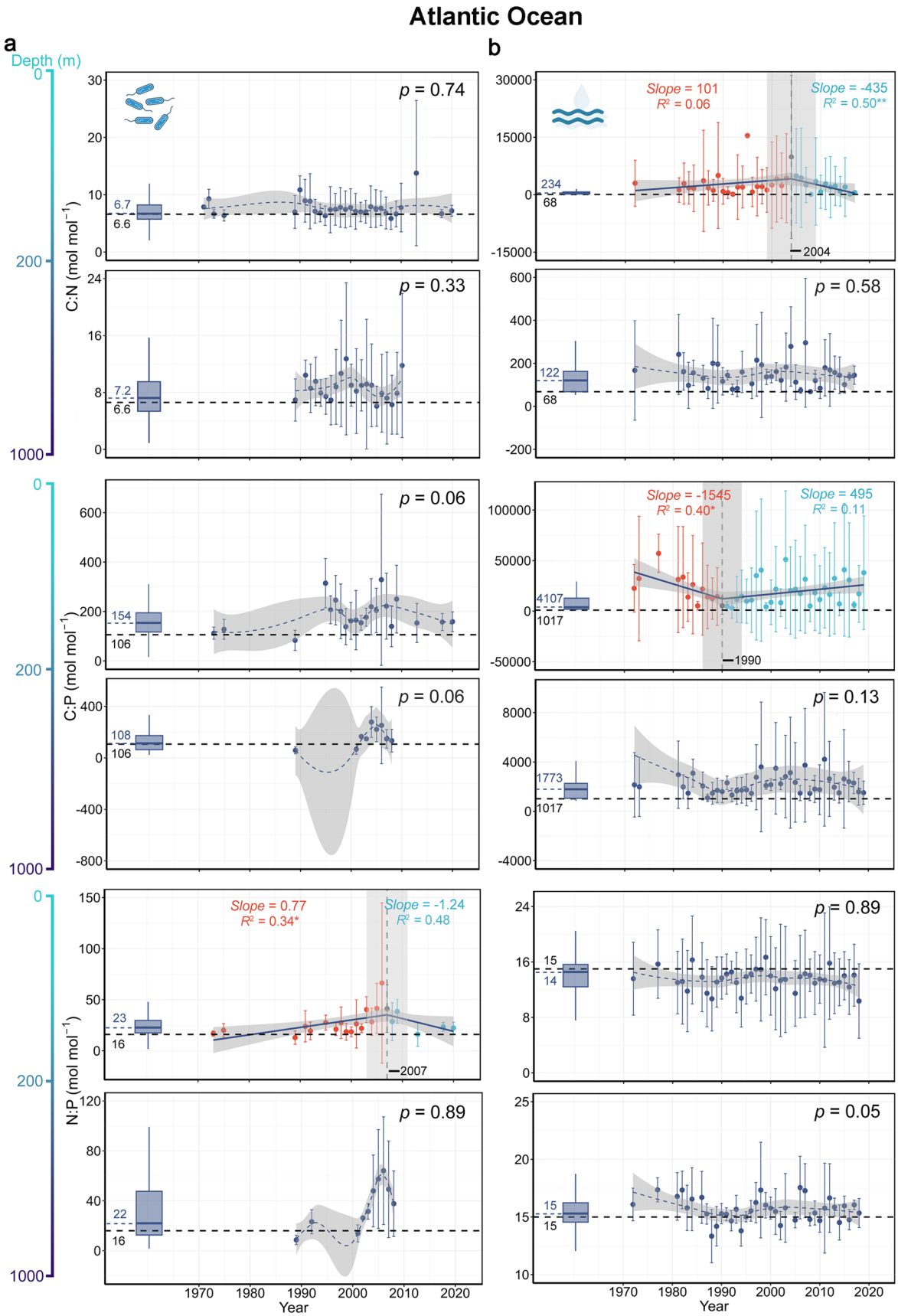

Extended Data Fig. 4 | See next page for caption.

https://doi.org/10.1038/s41561-025-01735-y

Extended Data Fig. 4 | Temporal trends in planktonic (a, n = 23788) and oceanic (b, n = 105541) ecological stoichiometry of the Atlantic Ocean. The boxplot represents the distribution of data for all years from 1970 to 2020. For the boxplot, the straight line in the center represents the median, or 2nd quartile (Q2), the top edge of the box represents the 3rd quartile (Q3), and the bottom edge of the box represents the 1st quartile (Q1). The black and blue dashed lines represent the Redfield ratio and the ecological stoichiometric ratio established in this study, respectively. The error bars represent the mean and standard deviation of the stoichiometric ratios for each year. The significance of the non-zero coefficients in the segmented model fitting is evaluated through a two-tailed t-test. If $p > 0.05$, it indicates that there is no obvious trend of change in the stoichiometric ratio over time. The shaded area of the fitted line represents the 95% confidence interval of the predicted values. The shaded area at the segmentation point represents the uncertainty of the time breakpoints, which is derived from the standard deviation of the breakpoint estimates across iterations based on resampling. *, $p < 0.05$; **, $p < 0.01$; ***, $p < 0.001$.

https://doi.org/10.1038/s41561-025-01735-y

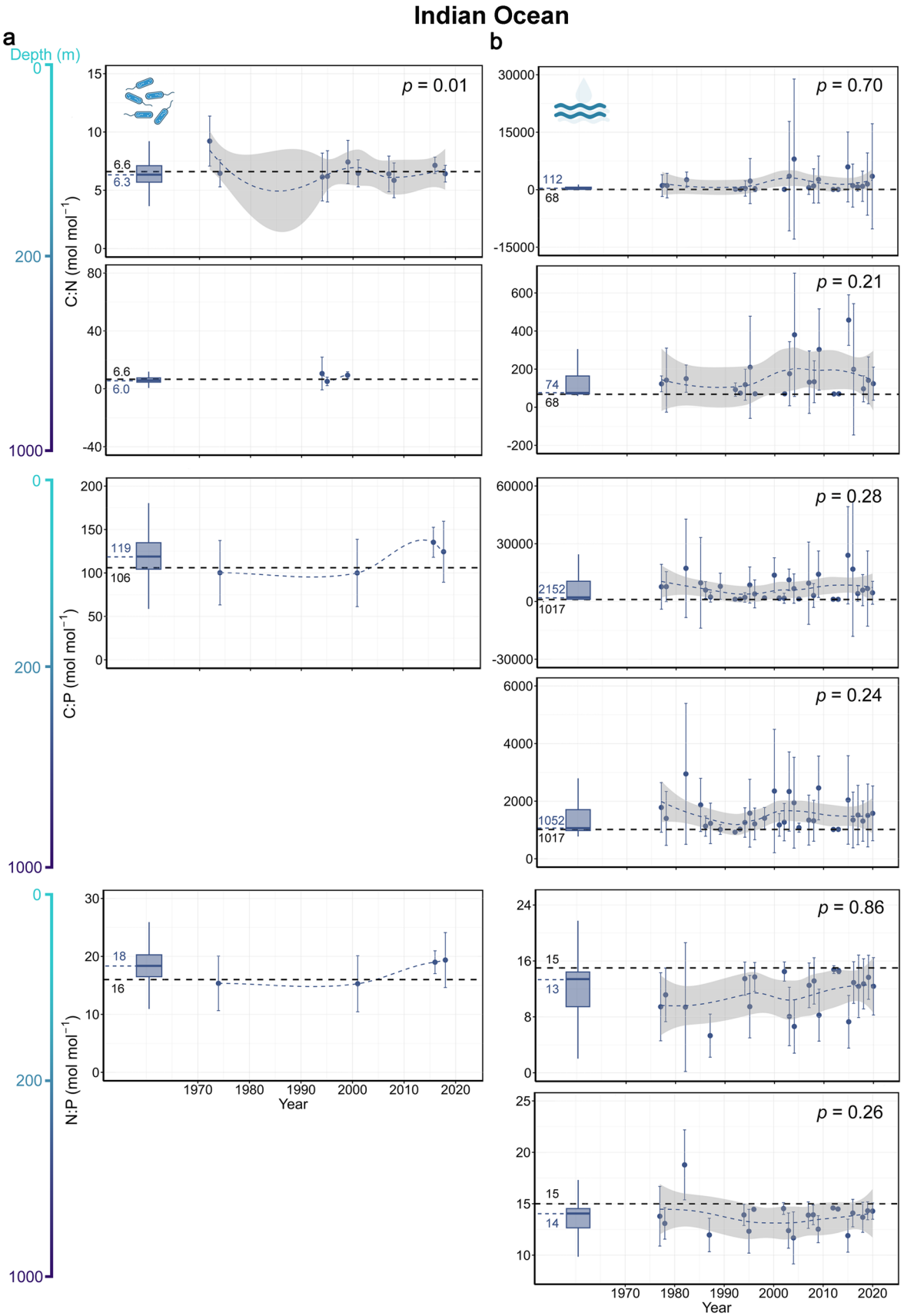

Extended Data Fig. 5 | See next page for caption.

https://doi.org/10.1038/s41561-025-01735-y

Extended Data Fig. 5 | Temporal trends in planktonic (a, n = 3612) and oceanic (b, n = 45558) ecological stoichiometry of the Indian Ocean. The boxplot represents the distribution of data for all years from 1970 to 2020. For the boxplot, the straight line in the center represents the median, or 2nd quartile (Q2), the top edge of the box represents the 3rd quartile (Q3), and the bottom edge of the box represents the 1st quartile (Q1). The black and blue dashed lines represent the Redfield ratio and the ecological stoichiometric ratio established in this study, respectively. The error bars represent the mean and standard deviation of the stoichiometric ratios for each year. The significance of the non-zero coefficients in the segmented model fitting is evaluated through a two-tailed t-test. If $p > 0.05$, it indicates that there is no obvious trend of change in the stoichiometric ratio over time. The shaded area of the fitted line represents the 95% confidence interval of the predicted values. The shaded area at the segmentation point represents the uncertainty of the time breakpoints, which is derived from the standard deviation of the breakpoint estimates across iterations based on resampling. *, $p < 0.05$; **, $p < 0.01$; ***, $p < 0.001$.

https://doi.org/10.1038/s41561-025-01735-y

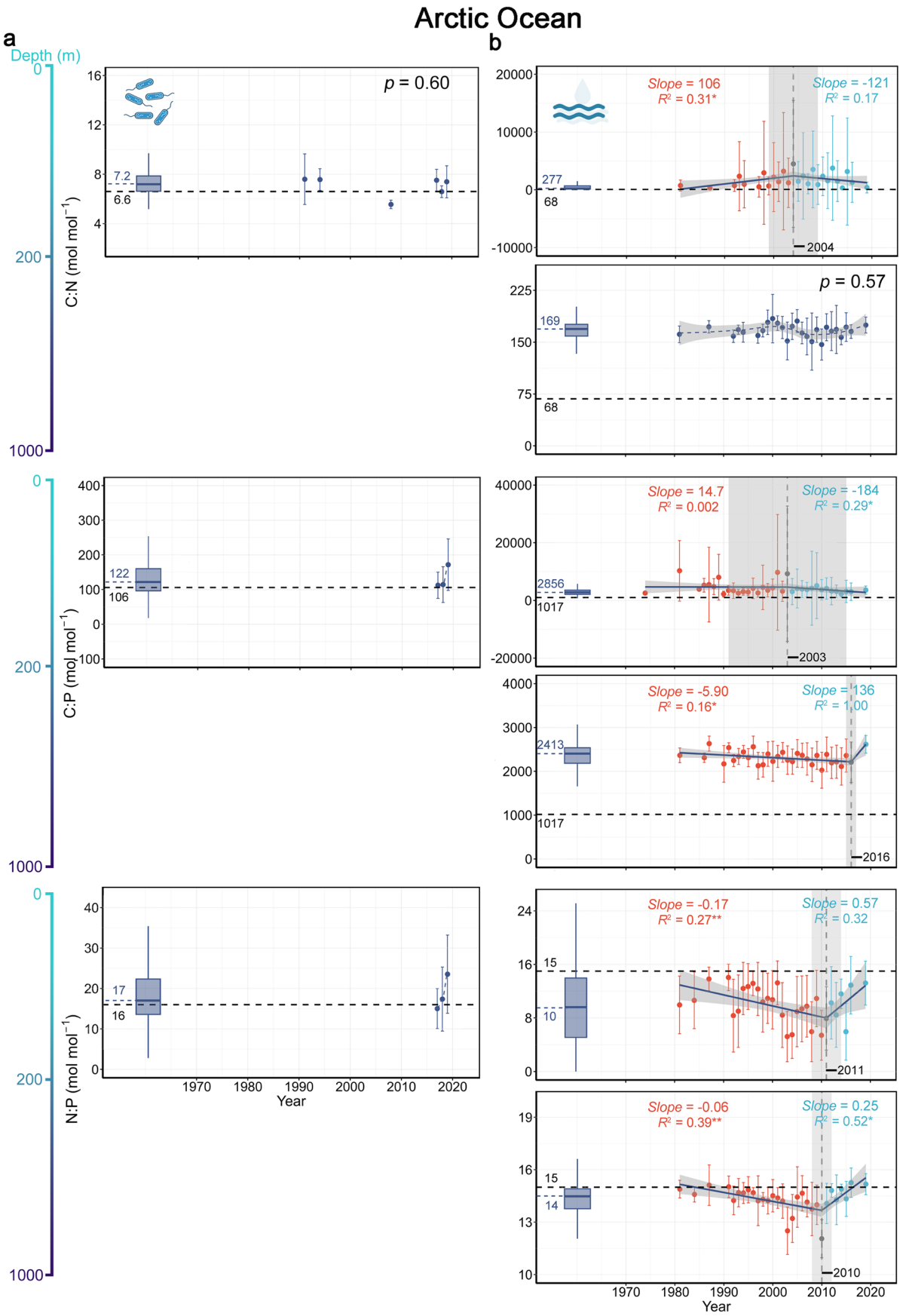

Extended Data Fig. 6 | See next page for caption.

https://doi.org/10.1038/s41561-025-01735-y

Extended Data Fig. 6 | Temporal trends in planktonic (a, n = 296) and oceanic (b, n = 59929) ecological stoichiometry of the Arctic Ocean. The boxplot represents the distribution of data for all years from 1970 to 2020. For the boxplot, the straight line in the center represents the median, or 2nd quartile (Q2), the top edge of the box represents the 3rd quartile (Q3), and the bottom edge of the box represents the 1st quartile (Q1). The black and blue dashed lines represent the Redfield ratio and the ecological stoichiometric ratio established in this study, respectively. The error bars represent the mean and standard deviation of the stoichiometric ratios for each year. The significance of the non-zero coefficients in the segmented model fitting is evaluated through a two-tailed t-test. If $p > 0.05$, it indicates that there is no obvious trend of change in the stoichiometric ratio over time. The shaded area of the fitted line represents the 95% confidence interval of the predicted values. The shaded area at the segmentation point represents the uncertainty of the time breakpoints, which is derived from the standard deviation of the breakpoint estimates across iterations based on resampling. *, $p < 0.05$; **, $p < 0.01$; ***, $p < 0.001$.

https://doi.org/10.1038/s41561-025-01735-y

Extended Data Table 1 | A summary of the global planktonic and oceanic ecological stoichiometric ratio of different sea areas across different depth ranges

Depth	Sea-water analyses	Sea areas	C:N (molar ratio)			C:P (molar ratio)			N:P (molar ratio)		
			Values (95% CI)	Redfield ratio	*p*	Values (95% CI)	Redfield ratio	*p*	Values (95% CI)	Redfield ratio	*p*
0-200	Plankton	Pacific	6.41(6.40-6.43)	6.63	***	144 (142-146)	106	***	20.9 (20.5-21.0)	16.0	***
		Atlantic	6.73 (6.70-6.76)		***	154 (153-156)		***	22.6 (22.5-22.9)		***
		Indian	6.35 (6.31-6.40)		***	119 (118-120)		***	18.3 (18.3-18.5)		***
		Arctic	7.18 (7.10-7.31)		***	122 (117-130)		***	17.0 (16.0-17.7)		***
	Ocean	Pacific	234 (228-238)	67.8	***	3975 (3875-4061)	1017	***	12.0 (12.0-12.0)	15.0	***
		Atlantic	234 (229-238)		***	4107 (4043-4173)		***	14.5 (14.5-14.5)		***
		Indian	112 (108-117)		***	2152 (2067-2250)		***	13.4 (13.3-13.4)		***
		Arctic	277 (271-283)		***	2856 (2840-2873)		***	9.66 (9.51-9.82)		***
200-1000	Plankton	Pacific	7.14 (7.03-7.25)	6.63	***	161 (140-180)	106	***	22.5 (20.5-25.0)	16.0	***
		Atlantic	7.17 (6.95-7.32)		***	108 (91.9-119)		*	22.0 (18.8-26.3)		***
		Indian	6.00 (5.80-6.23)		***						
		Arctic									
	Ocean	Pacific	77.2 (76.1-78.2)	67.8	***	1010 (1008-1012)	1017	***	13.9 (13.9-13.9)	15.0	***
		Atlantic	122 (121-123)		***	1773 (1757-1786)		***	15.3 (15.3-15.3)		***
		Indian	74.5 (73.6-76.1)		***	1052 (1050-1055)		***	14.0 (14.0-14.1)		***
		Arctic	169 (169-169)		***	2413 (2407-2419)		***	14.5 (14.5-14.5)		***
0-1000	Plankton	Pacific	6.45 (6.43-6.46)	6.63		144(142-147)	106	***	20.9 (20.6-21.1)	16.0	***
		Atlantic	6.75 (6.72-6.78)		***	153 (152-155)		***	22.6 (22.5-22.9)		***
		Indian	6,33(6.28-6.38)		***	119 (118-120)		***	18.3 (18.3-18.5)		***
		Arctic	7.18 (7.10-7.31)		***	122 (117-130)		***	17.0 (16.0-17.7)		***
	Ocean	Pacific	145 (143-148)	67.8	***	1406 (1397-1415)	1017	***	13.2 (13.1-13.2)	15.0	***
		Atlantic	156 (155-158)		***	2170 (2160-2182)		***	14.8 (14.7-14.8)		***
		Indian	94.8 (93.2-96.7)		***	1265 (1255-1277)		***	13.7 (13.6-13.7)		***
		Arctic	198 (198-200)		***	2559 (2553-2566)		***	12.7 (12.6-12.8)		***

The values for plankton and ocean are the median of the elemental ratios. Values in parentheses are 95% confidence intervals (CI). *, $p<0.05$; **, $p<0.01$; ***, $p<0.001$.